Bifunctional Pt-IrO_2 Catalysts for the Oxygen Evolution and Oxygen Reduction Reactions: Alloy Nanoparticles vs. Nanocomposite Catalysts

Jia Du[a], Jonathan Quinson[b], Damin Zhang[a], Francesco Bizzotto[a], Alessandro Zana[a], Matthias Arenz[a] *

[a] Department of Chemistry and Biochemistry, University of Bern, Freiestrasse 3, 3012 Bern, Switzerland

[b] Department of Chemistry, University of Copenhagen, Universitetsparken 5, 2100 Copenhagen Ø, Denmark

* corresponding author: matthias.arenz@dcb.unibe.ch

Abstract

In the present study different concepts for the development of bifunctional oxygen reduction reaction / oxygen evolution reaction (ORR / OER) electrocatalysts are explored and compared. Bifunctional ORR / OER catalysts are often suggested to improve the stability during startup and shutdown of fuel cells. Furthermore, they have been proposed for so-called unitized regenerative fuel cells (URFCs) that would allow a closed loop system to use and produce hydrogen on demand. We compare the electrocatalytic performance of conventional Pt_xIr_y alloy nanoparticles (NPs) with Pt – IrO_2 NP composites (nanocomposites), both immobilized onto a commercial carbon support. The Pt – IrO_2 nanocomposites thereby consist of a mixture of Pt NPs and IrO_2 NPs. By probing the electrocatalytic performance before and after exposing the electrocatalysts to accelerated degradation tests (ADTs) it is shown that the Pt – IrO_2 nanocomposite concept offers advantages but also some disadvantages over the conventional alloy concept. In particular it is shown that while the nanocomposites are initially less active for the ORR due to an interparticle effect, their performance is less affected by the ADTs. However, all tested catalysts experience a decline of the Ir / Pt ratio upon the ADTs treatment, highlighting the limiting value of Ir as OER catalyst for

startup-shutdown protection in fuel cells as well as the challenging stability requirements for URFCs.

Keywords
bimetallic electrocatalysts; nanocomposite electrocatalysts; alloy nanoparticles; accelerated degradation test; startup-shutdown degradation; fuel cells; unitized regenerative fuel cells;

1. Introduction

Electrochemical energy conversion is one of the main applications of electrocatalysis.[1–3] The most studied technologies and reactions are the electrochemical water splitting to produce hydrogen as an energy carrier as well as the re-conversion of such "green hydrogen" (provided the electricity is based on renewable sources such as wind or solar power) in fuel cells to deliver electricity on demand.[4–7] In addition, a number of new reactions such as electrochemical carbon dioxide reduction[8,9] or the production of valuable chemicals[10,11] recently received increasing attention. While the main application of fuel cells is often seen in the mobile automotive sector[12] with a recent focus shift to larger trucks,[13] also a great potential exists for applications such as power backup,[14] residential areas,[15] or range extenders for batteries.[16]

In proton exchange membrane fuel cells (PEMFCs) most conversion losses arise at the cathode where the oxygen reduction reaction (ORR) takes place.[17] The electrocatalyst of choice for the cathode currently consists of bimetallic Pt nanoparticles (NPs), mainly PtCo, immobilized onto a carbon support.[18,19] The alloying optimizes the adsorption strength of the ORR reaction intermediates (O_{ad}, OH_{ad}, OOH_{ad}) on Pt and thus the ORR rate.[20,21] However, also other Pt-based bimetallic electrocatalysts are investigated for PEMFCs like PtIr.[22] Ir is equally scarce and recently even more expensive than Pt.[23] The motivation behind developing PtIr catalysts is not necessarily

the optimization of the binding energy of reaction intermediates but rather the fact that Ir-oxide is an active catalyst for the oxygen evolution reaction (OER).[24,25] Bifunctional ORR / OER electrocatalysts are suggested to improve the stability of PEMFCs cathode catalysts since under high potential excursions reached during startup and shutdown, the OER competes with and thus mitigates the oxidation of the carbon support to carbon dioxide, the latter being extremely detrimental to the catalyst stability. Furthermore, bifunctional ORR / OER electrocatalysts were suggested for so-called unitized regenerative fuel cells (URFCs). URFCs are a concept for a closed loop system that can use hydrogen fuel to produce electricity as well as re-generate the hydrogen fuel when connected to an external energy source.[26–28] URFCs allow two operation modes, a charge (electrolyzer) mode and a discharge (fuel cell) mode. To sustain both operation modes bifunctional catalysts are required. A distinction, however, can be made between two concepts, the constant-gas (CG) and the constant-electrode (CE) configuration.[28] In the CG configuration, the URFC consists of an oxygen electrode to sustain the ORR and OER and a hydrogen electrode for the hydrogen oxidation and the hydrogen evolution reactions (HOR/HER). By comparison, in the CE configuration the two electrodes are a HOR/OER and an ORR/HER electrode. The advantages of the classical CG configuration are that H_2 and O_2 mixing is avoided and fast switching between the two modes is possible.[28] In the CG configuration using proton conducting membranes most approaches for URFCs use bifunctional catalysts composed of Pt and IrO_2. Thereby different types have been investigated ranging from simple mixtures of Pt and IrO_2[29] to Pt_xIr_y alloys,[30] Pt NPs deposited onto IrO_2 black[31], nickel-platinum/cobalt-iridium two-dimensional (2D) nanoframes,[32] or IrO_2 deposited onto Pt black.[33] More recently also composite materials are discussed.[34] One of the main challenges for employing URFCs are the stability requirements[35] of the catalyst at these harsh conditions changing from oxidative to reductive conditions.

In the present study, we use our previously introduced toolbox approach[36–39] to compare different concepts for bifunctional ORR / OER electrocatalysts. Pt_xIr_y alloy NPs as well as composites consisting of separated Pt and IrO_2 NPs (Pt – IrO_2 nanocomposites) are investigated; both systems in immobilized form using a commercial carbon support. Carbon supported monometallic Pt NPs serve as a reference system. The electrocatalysts are probed for their electrocatalytic performance for the ORR and OER. Furthermore, accelerated degradation tests (ADTs) are performed exposing the electrocatalysts repeatedly to a series of reductive and oxidative currents. The influence of these ADTs treatments is examined with respect to the type of catalysts (alloys vs. nanocomposites), electrochemically active Pt surface area (Pt ECSA) loss as well as ORR and OER activity. In addition, the influence of ADTs treatments on the catalyst composition is probed.

2. Experimental:

Chemicals and gases

The following chemicals were used for catalyst synthesis and characterization: ethylene glycol (EG, 99.8%, Sigma Aldrich), sodium hydroxide (NaOH, 98.9%, Fisher Chemical), hexa-chloroplatinic (IV) acid hexahydrate ($H_2PtCl_6 \cdot 6H_2O$, 99.9%, Alfa Aesar), iridium (III) chloride ($IrCl_3 \cdot xH_2O$, Sigma Aldrich, >99.8%), 30% hydrochloric acid (HCl, Suprapur, Merck), 65% nitric acid (HNO_3, Suprapur, Merck) and acetone (99.5+%, Alfa Aesar). Commercial carbon black, Vulcan XC72R was employed as carbon support in the catalyst synthesis. Ultrapure water (resistivity>18.2 MΩ·cm, total organic carbon (TOC) <5 ppb) from a Milli-Q system (Millipore) was used for acid/base dilutions, catalyst ink formulation and electrochemical cell cleaning. Isopropanol (IPA, 99.7+%, Alfa Aesar), 70% perchloric acid ($HClO_4$, Suprapur, Merck), potassium hydroxide hydrate ($KOH \cdot H_2O$, Suprapur, Merck) were used for the catalyst ink

formulation and electrolyte preparation. The following gases from Air Liquide were used for electrochemical measurements: Ar (99.999%), O_2 (99.999%), and CO (99.97%).

Synthesis of supported monometallic Pt NPs, Pt_xIr_y alloy NPs and Pt – IrO_2 nanocomposites

Bifunctional electrocatalysts were synthesized *via* the toolbox method we previously reported.[36–39] The synthesis approach consists of two main steps: NPs were first prepared assisted by a microwave reactor *via* an alkaline EG route, and then in the second step the NPs were immobilized onto a carbon support.

The colloidal Pt or Ir NP synthesis in alkaline EG was conducted by mixing 5 mL NaOH EG solution (0.4 M) with 5 mL $H_2PtCl_6 \cdot 6H_2O$ or $IrCl_3 \cdot xH_2O$ EG solution (0.04 M) in a microwave reaction vessel and heating the mixture to 160 °C for 3 minutes in the microwave reactor to obtain colloidal Pt or Ir NPs in EG with a concentration of 3.9 $g_{Pt}\ L^{-1}$ and 3.85 $g_{Ir}\ L^{-1}$, respectively. Pt_xIr_y alloy NPs were synthesized according to a previously reported method,[40] for PtIr alloy NPs, 2.5 mL $H_2PtCl_6 \cdot 6H_2O$ EG solution (0.04 M) and 2.54 mL $IrCl_3 \cdot xH_2O$ EG solution (0.04 M) were mixed with 5.04 mL NaOH EG solution (0.4 M), the mixture was heated to 160 °C for 3 minutes in the microwave reactor to obtain alloyed colloidal PtIr NPs in EG with a concentration of 1.936 $g_{Pt}\ L^{-1}$ and 1.936 $g_{Ir}\ L^{-1}$. For the preparation of $PtIr_2$ alloy NPs, the synthesis procedure was similar but with different Pt and Ir precursor contents, i.e. 1.5 mL $H_2PtCl_6 \cdot 6H_2O$ EG solution (0.04 M) and 3.05 mL $IrCl_3 \cdot xH_2O$ EG solution (0.04 M) were mixed with 4.55 mL NaOH EG solution (0.4 M) followed by heating the mixture to 160 °C for 3 minutes in the microwave reactor to obtain colloidal $PtIr_2$ alloy NPs in EG with a concentration of 1.288 $g_{Pt}\ L^{-1}$ and 2.576 $g_{Ir}\ L^{-1}$. All colloidal NP suspensions looked dark brown after synthesis.

In order to immobilize the NPs on carbon, 1 M HCl was added to the colloidal NP suspension ($V_{HCl} : V_{NPs} = 3 : 1$) inducing particle flocculation. The mixture was thereafter centrifuged at 5000 rpm for 10 minutes once, the supernatant was discarded, and the floc was re-dispersed in acetone to obtain NPs acetone solution with the same concentration as before the flocculation in EG. To immobilize the monometallic Pt NPs, 5.5 mg carbon (Vulcan XC72R) was dispersed in 10 mL acetone, the carbon suspension was sonicated with a horn sonicator (QSONICA sonicator, 500 W, 50 kHz, with alternation of 1 s sonication and 1 s resting) until it showed stable dispersion (~3 minutes), then Pt NPs acetone solution of 352 µL or 940 µL was added and further sonicated for 10 minutes (during which the vial was immersed in ice water to avoid overheating of the dispersion), finally, the acetone was evaporated from the mixture with the help of a rotary evaporator (r.t., 200 mbar) until the catalyst was completely dried and the respective 20 wt. % Pt/C or 40 wt. % Pt/C were obtained. The same procedure was employed to obtain immobilized Pt_xIr_y alloy NPs. In brief, the same amount (5.5 mg) of carbon was dispersed in 10 mL acetone, after sonication, the PtIr alloy NPs dispersed in 710 µL acetone or the $PtIr_2$ alloy NPs dispersed in 1068 µL acetone were added, further sonicated for 10 minutes, and the solvent evaporated in a rotary evaporator, obtaining the PtIr alloy/C or $PtIr_2$ alloy/C catalysts. Concerning the supported Pt – IrO_2 nanocomposites, Pt NPs acetone solution and Ir NPs acetone solution were added to the sonicated carbon acetone suspension (5.5 mg in 10 mL acetone) one by one: first 352 µL Pt NPs acetone solution, then 357 µL or 714 µL Ir NPs acetone solution, respectively, the mixture was further sonicated and the solvent evaporated, obtaining nanocomposites with Pt to Ir NP ratio of 1 : 1 and 1 : 2 based on metal weight. The Pt weight loading on the carbon support thereby is fixed to 20 wt. %.

Transmission electron microscopy (TEM) and energy dispersive X-ray spectroscopy (EDX)

For the TEM analysis, a Jeol 2100 transmission electron microscope operated at 200 kV equipped with an EDX detector was used. The samples were prepared by dropping the catalyst dispersion diluted in ethanol on carbon coated copper TEM grids (Quantifoil). For TEM after electrochemical treatments, the samples were collected from the rotating disk electrode (RDE) for preparation of TEM grids. Images were recorded at different magnifications (at least x300 000, x400 000, x500 000) in at least three randomly selected areas. The composition of the samples was evaluated by measuring the relative ratio of Pt and Ir in at least three and typically five different randomly selected areas.

Inductively Coupled Plasma Mass Spectrometry (ICP-MS)

The Pt loading in the Pt/C catalysts was determined via an indirect Pt proof.[41] The actual content of Pt and Ir in the bifunctional catalysts was evaluated by ICP-MS (NexION 2000 ICP-MS). The Ir loading in the bifunctional catalyst was indirectly evaluated by measuring the Ir content lost during the immobilization procedure. That is the amount of Ir NPs remaining in the supernatant after flocculation by HCl as well as the Ir NPs remaining in the re-dispersing solvent acetone were determined by ICP-MS after dissolution in aqua regia (volume ratio of HCl : HNO_3 = 3 : 1). The volume was adjusted to 20 mL with milli-Q water. The ICP-MS was equipped with a cyclonic spray chamber and a PFA-nebulizer. The RF power for the plasma was held at 1300 W with a gas flow of 15 L min^{-1}.

Electrochemical measurements

All electrochemical measurements were performed using a computer controlled potentiostat (ECi 200, Nordic Electrochemistry) and a glass cell equipped with three electrodes. A 5 mm mirror-polished glassy carbon (GC) disk embedded in a Teflon tip (homogeneous thin films of Pt based

catalysts on GC were prepared by pipetting different amount of each catalyst ink on GC to lead the same loading of Pt (10 µg cm^{-2}) and drying in air) was used as the working electrode (WE) and a platinum wire as counter electrode (CE). All potentials were measured with respect to a reversible hydrogen electrode (RHE). The electrolyte was 0.1 M $HClO_4$ prepared by diluting 70% $HClO_4$ with milli-Q water. The effective solution resistance was compensated to below 3 Ω via an analog positive feedback scheme. Prior to all electrochemical measurements and accelerated degradation tests (ADTs), the electrolyte was de-aerated by purging with Ar, the supported monometallic Pt NPs were cleaned by potential cycling between 0.05 V_{RHE} and 1.20 V_{RHE} at a scan rate of 500 mV s^{-1} until a stable cyclic voltammograms (CVs) could be observed, the supported Pt_xIr_y alloy NPs and Pt – IrO_2 nanocomposites were cleaned by potential cycling between 0.10 V_{RHE} and 0.30 V_{RHE} at a scan rate of 100 mV s^{-1} for 20 cycles (in order not to oxidize Ir to obtain the exact value of the ECSA originating from Pt as well as Ir; once Ir is oxidized, the CO stripping method for the Ir ECSA determination does not work as Ir oxide does not adsorb CO).[42]

After cleaning, for each bimetallic catalyst layer the following automized measurement procedure was applied using a macro-script of the potentiostat software: CO stripping, Ir activation, CO stripping, ORR activity determination, OER activity determination, ADT treatment, ORR activity determination, OER activity determination, CO stripping. The activities are determined with respect to the metal mass (mass activity (MA)) as well as with respect to the electrochemically active surface area (specific activity (SA)).

Ir activation was performed by holding the potential at 1.60 V_{RHE} for 8 minutes followed by cycling the electrode potential between 0.05 V_{RHE} and 1.20 V_{RHE} for around 100 cycles to clean the catalyst surface until a stable CV with the typical features of Pt was obtained.

The ECSA was determined *via* the oxidation charge in CO monolayer stripping experiments.[43] Two different ECSAs were determined, the ECSA of the pristine catalyst in the reduced state and the ECSA after Ir activation. In the reduced state Ir as well as Pt adsorb CO and the charge from the CO monolayer stripping relates to the total (Ir + Pt) ECSA, whereas after activation the oxidized Ir NPs do not adsorb CO and only the Pt ECSA is determined as demonstrated in previous studies showing that after electrochemical activation the Ir NPs cannot be easily reduced again;[42] even after holding at low potentials in hydrogen atmosphere for 30 min only around 10 % of the initial Ir surface area was determined in CO stripping. To determine the total ECSA, the electrode was held at 0.15 V_{RHE} in a CO-saturated electrolyte for 2 minutes. Thereafter the electrolyte was saturated with Ar to replace the excess CO in the electrolyte. The adsorbed CO monolayer was oxidized to CO_2 by scanning the potential from 0.15 to 1.10 V_{RHE} and 1.40 V_{RHE}, respectively, for Pt/C and the different bifunctional PtIr catalysts. The scan rate of 50 mV s^{-1}. After activating the different bifunctional PtIr catalysts, a second CO stripping curve was recorded in the same manner, however at a reduced potential window between 0.15 and 1.10 V_{RHE}. To calculate the Pt ECSA a reference monolayer oxidation charge value of 396 µC cm_{Pt}^{-2} was used[44] and for Ir 358 µC cm_{Ir}^{-2}.[45] The Ir surface area was estimated by subtracting the Pt surface area from the total surface area, leading to nominal Ir surface areas up to 225 m^2 g_{Ir}^{-1} for all the different PtIr catalysts, which even slightly succeeds the ECSA of Ir nanoparticles deposited onto a planar support.[42] The thus determined nominal Ir surface area might be slightly over-estimated due to currents related to irreversible (hydro) oxide formation on Ir.[46] 225 m^2 g_{Ir}^{-1} corresponds to an average particle size about 1.2 nm, which is in agreement with the particle size determined in small angle X-ray scattering but slightly lower than the average size determined in TEM.[42] In addition, this estimation disregards the shielding of parts of the particle surface due to the particle support interface. The

likely overestimation of the Ir surface area leads to an underestimation of the specific OER activity but does not influence any of the conclusions made. Representative CO stripping curves for a pristine and activated Pt – IrO_2 nanocomposite are presented in Figure S1. It can be clearly seen that the area under the CO stripping curve is significantly higher in the pristine nanocomposite catalyst (Pt plus Ir surface area) as compared to after activation (Pt surface area).

In order to determine the ORR activity, measurements were conducted in O_2 saturated electrolyte at a scan rate of 50 mV s^{-1} and a rotation speed of 1600 rpm.[43] The polarization curves were corrected by background subtraction (CVs recorded in Ar saturated electrolyte at the identical scan rate). The specific activity was analyzed and compared at 0.90 V_{RHE} from positive going scan direction on polarization curve normalized by Pt area. The mass activity was analyzed and compared at 0.90 V_{RHE} normalized by Pt content and total metal content, respectively.

In order to determine the OER activity, the potential was scanned between 1.00 V_{RHE} and 1.70 V_{RHE} at a scan rate of 10 mV s^{-1} and a rotation speed of 1600 rpm. The OER specific activity was analyzed based on the current at 1.50 V_{RHE} during the positive going scan direction normalized by the total surface area, while for the mass activity the current at 1.50 V_{RHE} was normalized by Pt content (Pt/C catalysts), Ir content and total metal content, respectively (PtIr bimetallic catalysts).

Accelerated Degradation Tests (ADTs) protocol

The stability of the catalysts was scrutinized employing ADTs with a current control protocol. The protocol was developed based on the simulation of load cycling and is mainly designed to probe startup-shutdown conditions in fuel cells for which bifunctional ORR/OER catalysts have been suggested. A similar degradation protocol for this purpose was employed in previous work of Dahn and co-workers.[47] The degradation test was conducted in the O_2-saturated $HClO_4$ electrolyte

maintaining a rotation of 1600 rpm. The current was stepped between 0 and -5 mA cm_{geo}^{-2}, which is roughly the diffusion limited current during ORR in a RDE measurement at 1600 rpm, with a rest time of 1 s. This procedure was repeated for 5 times followed by a current step to 1 mA cm_{geo}^{-2} for one second. The above procedure was regarded as a basic unit and this unit was repeated for 300 times, as schematized in **Figure 1**. The ECSA, ORR activity and OER activity were recorded before and after applying the ADT. ADTs solely focusing on URFC application usually employ an equal number of excursions to oxidizing and reducing conditions.

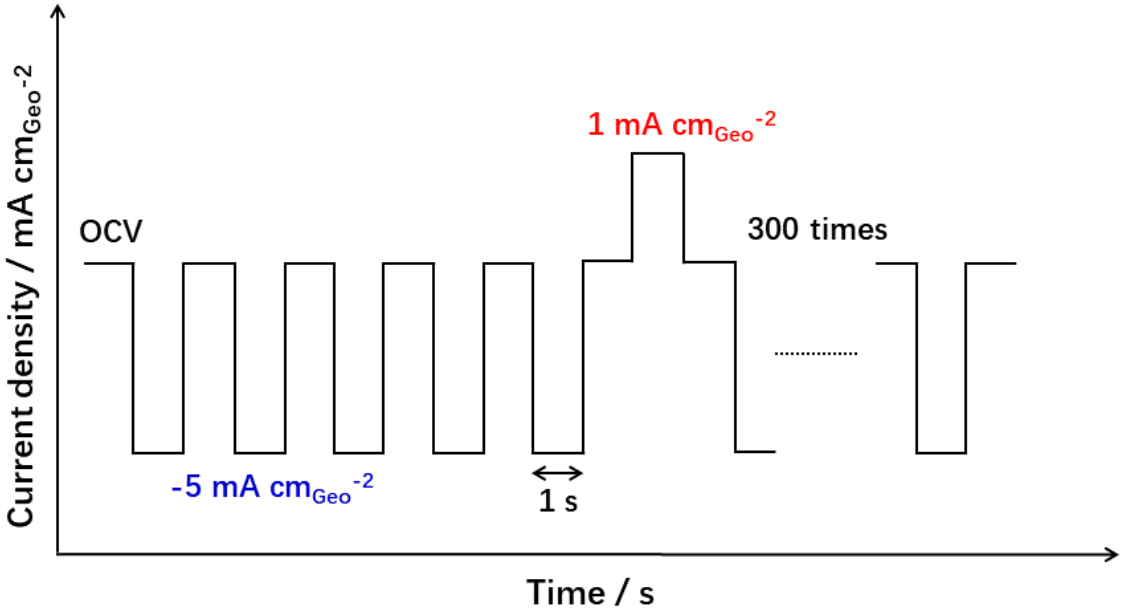

Figure 1. Scheme of the ADTs protocol applying steps between different current density. All measurements are performed in oxygen saturated 0.1 M $HClO_4$ solution at room temperature applying a rotation rate of 1600 rpm.

3. Results and discussion

As outlined in the introduction the aim of this study is to utilize our colloidal toolbox approach[36–39] to compare the performance and stability of two different concepts for bifunctional ORR / OER catalysts, i.e. Pt_xIr_y alloy NPs and nanocomposites composed of a mixture of monometallic Pt and Ir NPs. The catalysts were investigated after supporting on commercial high surface area carbon

support (Vulcan XC72R). For both approaches, two nominal weight compositions were prepared, i.e. Pt : Ir = 1 : 1 and Pt : Ir = 1 : 2 (due to the very similar molecular weights of Pt and Ir, i.e. 195.084 u and 192.217 u, in the following we do not explicitly distinguish between weight and atomic ratios). For each bifunctional catalyst, the Pt loading on the carbon support was kept at 20 wt. %. This resulted in nanocomposites with 20 wt. % Pt and 20 wt. % Ir NPs and 20 wt. % Pt and 40 wt. % Ir NPs on carbon as well as Pt_xIr_y alloy NPs that follow the same composition and metal weight as the nanocomposites. Monometallic Pt NPs with 20 and 40 wt. % loading served as benchmark. In the following the catalysts are denominated as 20 % Pt/C, 40 % Pt/C, Pt + Ir/C, Pt + 2 Ir/C, PtIr /C, and $PtIr_2$/C.

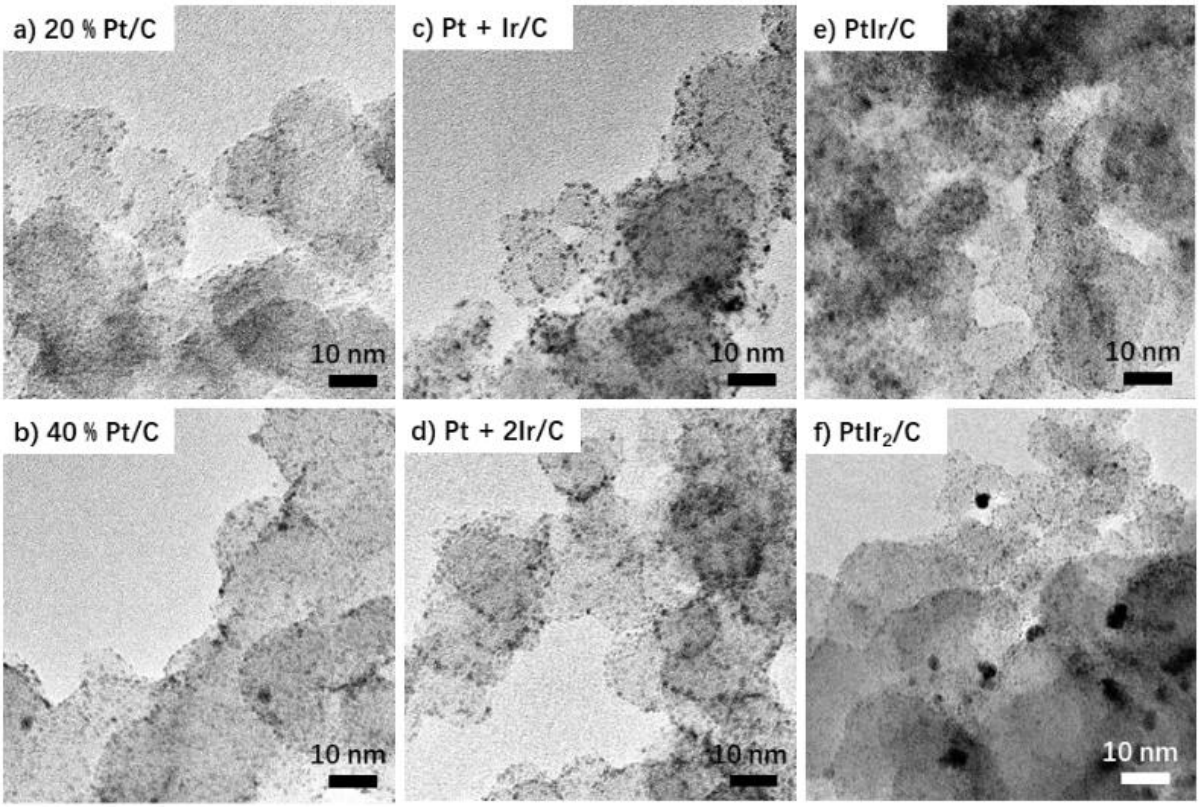

Figure 2. TEM micrographs of the as prepared catalyst samples. (a, b) Supported monometallic Pt NPs with 20 and 40 wt. % loading, respectively; (c, d) Supported Pt – Ir nanocomposites with 20 - 20 wt. % and 20 - 40 wt. % loading, respectively; (e, f) Supported PtIr alloy and $PtIr_2$ alloy NPs with the same metal loading as the nanocomposites.

We start the discussion with the physical characterization of the as prepared catalysts. In Figure 2 representative TEM micrographs of each catalyst are presented. It can be seen that the NPs are round in shape and well-dispersed on the carbon support. The size (diameter) of the individual Pt, Ir, and Pt_xIr_y NPs is in the range of 1 – 3 nm. For the monometallic and nanocomposite catalysts an increase in total metal loading from 20 to 40 wt. % (Pt/C, Figure 2a, b) and from 40 to 60 wt. % (Pt + Ir/C and Pt + 2 Ir/C, Figure 2c, d) leads to a slight increase in NP agglomeration. The fact that the Pt ECSA determined by CO stripping of the individual catalysts deviates less than 10 % from each other, see Table S2, confirms that the agglomeration is not significant. An EDX analysis of the nanocomposite catalysts further indicates that nominal (Pt : Ir of 1 : 1 and 1 : 2, respectively) and obtained compositions (Pt : Ir of 1.08 : 0.92 and 1.00 : 2.00, respectively) are in good agreement, see Table S4. The results therefore demonstrate the true nature of the nanocomposites with a mix of individual Pt and Ir NPs immobilized on the carbon support. By contrast in the case of the Pt_xIr_y alloy NPs, only the PtIr alloy (1 : 1 ratio at 40 wt. % total metal loading) contains the targeted metal ratio, see EDX analysis in Table S4. An increase to a nominal Pt : Ir ratio of 1 : 2 (associated with an increase in total metal loading on the support to 60 wt. %; $PtIr_2$/C sample), leads to a deviation of the established composition from the nominal one: a Pt : Ir composition of 0.90 : 1.10 is determined by EDX significantly deviating from the targeted 1 : 2 ratio. The large deviation from the nominal composition indicates that the mixing of Pt and Ir during the particle formation is insufficient. In addition, the formation of some agglomerated NPs on the carbon support can be seen in the TEM micrograph in Figure 2. However, the Pt ECSA is not largely affected by these agglomerates, see Table S2, while the overall metal area before the formation of the Ir-oxide phase is lower on the $PtIr_2$/C than on the Pt + 2Ir/C catalyst (the ratio between Pt and

Ir and their loading on the electrode are the same), Figure S1b. Last but not least, the results show that for this specific example of bimetallic catalysts, the catalyst composition can be more accurately tuned using a nanocomposite approach than in an alloying approach.

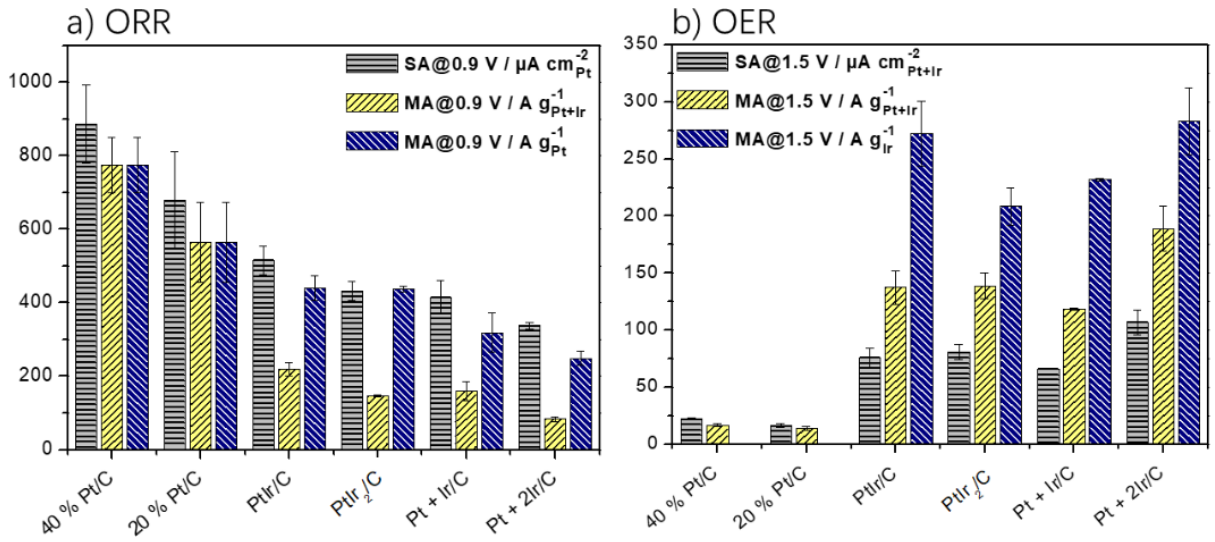

Figure 3. Comparison of the electrochemical activity of supported monometallic Pt NPs, Pt_xIr_y alloy NPs and Pt – IrO_2 nanocomposites before the ADT. a) ORR performance and b) OER performance. The ORR activity is determined with a scan rate of 50 mV s^{-1} and 1600 rpm applying a potential range of 0.05 - 1.10 V_{RHE}, while the OER activity is determined with a scan rate of 10 mV s^{-1} and 1600 rpm applying a potential range of 1.00 - 1.70 V_{RHE}. Concerning the OER performance of the Pt/C catalysts, the mass activity normalized to the total metal content equals the mass activity normalized to the Pt content. All measurements are performed at room temperature. As error, the standard deviation from three measurements on different catalyst films is given.

As discussed in the introduction, bifunctional oxygen catalysts that can catalyze the ORR as well as the OER are suggested to mitigate the degradation during startup and shutdown of fuel cells and are required for URFCs in CG configuration. Therefore, we evaluated the specific activity and mass activity for the ORR as well as the OER. Concentrating first on the ORR activities, Figure 3a, it should be noted that Ir-oxide[48] is not active for the ORR (in order to form bifunctional catalysts, the Ir was activated to Ir-oxide, see experimental section). As a consequence, the specific activity of the ORR is normalized to the Pt ECSA, whereas the mass activity of the ORR is given

based on normalization to the Pt mass as well as the total metal mass (Pt and Ir) to account for the fact that the mass activity is mainly used to account for the catalyst cost for a certain reaction. The results clearly show that the addition of Ir to the catalyst decreases the specific activity as well as the mass activity of the ORR; independent of normalization and regardless if a nanocomposite or alloy catalyst is prepared. This is a particularly interesting finding for the specific activity of the nanocomposite catalysts. As the specific activity is normalized to the Pt ECSA, which is not affected by the co-immobilization of the Ir NPs, see Table S1, a constant specific activity would be expected in case there is no electronic particle – particle interaction. Instead the results indicate that the electronic properties of the Pt NPs are affected by the adjacent Ir-oxide NPs. These particle – particle interactions may arise due to direct contact between Pt and Ir-oxide particles[31,32,35] or by reducing the interparticle distance to very small distances.[49–51] As an example of the former, it has been that the deposition of Pt nanoparticles onto an IrO_x support leads to a lattice contraction and an inhibition of the H_{upd} region of Pt.[31,52] The fact that no H_{upd} region is observed points to particle – particle interactions due to the particle proximity effect . This phenomenon so far was only observed for monometallic Pt clusters and NPs. In these cases a decrease in the interparticle distance lead to the enhancement of the ORR due to a reduced oxophilicity as well as a reduced Pt dissolution.[49–51] This is in line with the results obtained in the present work for monometallic Pt NPs. The ORR specific activity for the 40 % Pt/C as compared to the 20 % Pt/C is increased, i.e. 886 ± 50 µA cm_{Pt}^{-2} *vs.* 679 ± 132 µA cm_{Pt}^{-2} (Table S1). As the ECSA of both catalysts is very similar, the difference in specific activity directly translates into a corresponding difference in mass activity, i.e. 774.5 ± 74.5 A g_{Pt}^{-1} and 564.5 ± 109.4 A g_{Pt}^{-1}, respectively (Table S1). By comparison, the ORR on Pt seems to be inhibited by the adjacent Ir-oxide NPs. According to the Sabatier principle for the ORR,[53] this finding indicates an increase in oxophilicity of the Pt NPs

due to Pt – IrO_2 particle – particle interactions. For the Pt + 2Ir/C nanocomposite a specific activity of 338 ± 9 µA cm_{Pt}^{-2} and a mass activity of 249 ± 18.3 A g_{Pt}^{-1} were determined, see Table S1, which is only half the activity of the monometallic 20 % Pt/C catalyst.

It should be noted that the Pt_xIr_y alloy NPs exhibit a decreased ORR performance as well, both in Pt area normalized ORR activity and mass normalized ORR activity, see Table S1. The results therefore show that the different bifunctional ORR / OER catalysts suffer from ORR inhibition due to the addition of Ir (IrO_2) to the catalyst.

We next studied the OER performance of the bifunctional catalysts. Thereby we probed the OER activity based on the oxidation currents observed at 1.50 V_{RHE} in linear scan voltammetry (LSV) measurements. As Pt is not very active for the OER,[54] see Figure 3b, the monometallic Pt catalysts serve only as a comparison. It is seen that, as expected, the OER performance is considerably boosted by the introduction of activated Ir (IrO_2). Among the investigated catalysts, the Pt + 2Ir/C shows the highest specific activity for the OER, which in a URFC may compensate the lower activity of this catalyst for the ORR. For the other three catalysts, only a small difference in specific activity between the supported Pt_xIr_y alloy NPs and the Pt – IrO_2 nanocomposites is seen. The same trend is observed for the mass activity normalized to the total metal loading. Interestingly, normalizing the mass activity to the Ir loading, which can be considered the only active component for the OER, the trend slightly changes. The mass activity for PtIr/C catalyst, 272 ± 28.4 A g_{Ir}^{-1} becomes almost the same as the mass activity for the Pt + 2Ir/C sample, 283 ± 29.2 A g_{Ir}^{-1} (Table S1).

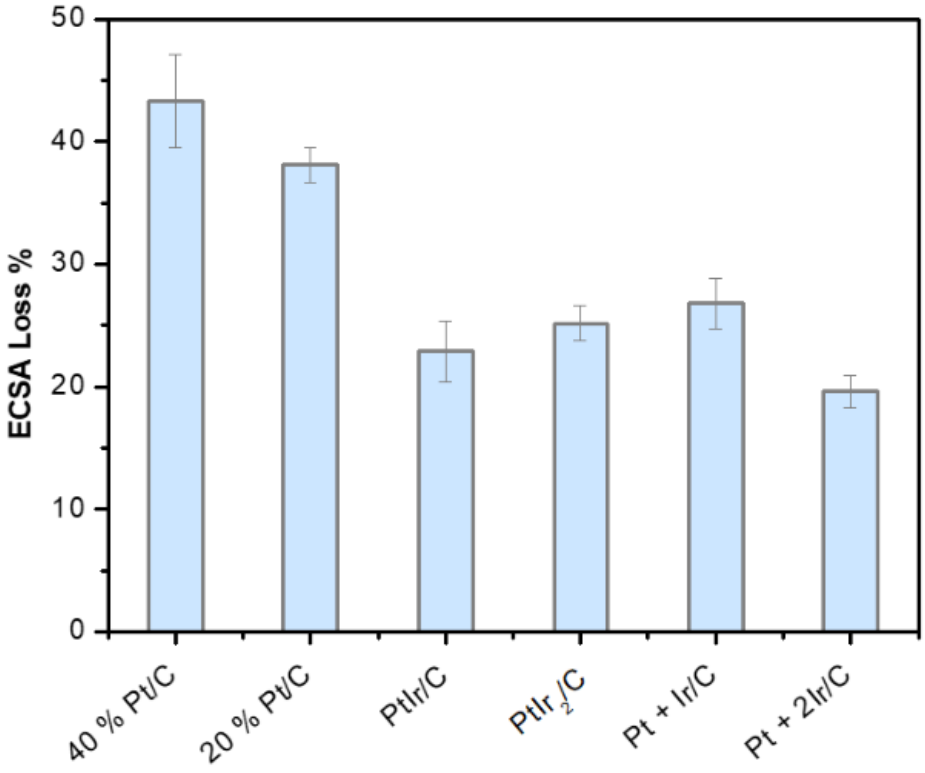

Figure 4. Comparison of the loss in electrochemically available Pt surface area for the supported monometallic Pt NPs, Pt_xIr_y alloy NPs and Pt – IrO_2 nanocomposites after an ADT with a current control protocol. As error, the standard deviation for three measurements on different catalyst films is given.

Overall, the differences in pristine OER activity between the catalysts are relatively small and no specific bifunctional catalyst stands out as most promising and preferred candidate for future deployment. A different conclusion is reached when the stability and resulting changes in performance are considered. The stability of the catalysts was evaluated by employing an ADT based on a current control protocol, i.e. fixed currents were applied instead of the conventional potential control. To take into account the bifunctional nature of the catalysts, reductive as well as oxidative currents were applied, albeit the oxidative currents were limited to avoid extensive carbon corrosion. The stability determination based on the loss in electrochemically available Pt surface area determined by CO stripping is summarized in Figure 4. Representative CO stripping curves for all catalysts before test (BOT) and end of test (EOT) are shown in Figure S2. In FigureS5

TEM micrographs of the degraded catalysts are shown. Based on the Pt ECSA loss, one can clearly state that Ir not only increases the OER activity but also boosts the stability of the catalysts. The ECSA loss for supported Pt_xIr_y alloy NPs and the Pt – IrO_2 nanocomposites is in the range between 19.6 ± 1.3 and 26.8 ± 2.1 %, which is roughly half of the ECSA loss seen without Ir, i.e. 38.1 ± 1.4 % for 20 % Pt/C and 43.3 ± 3.8 for 40 % Pt/C, see also Table S2. Furthermore, as a general trend, the ECSA loss seems to decrease with the Ir content. The catalyst stability can also be analyzed based on the CVs recorded in Ar saturated electrolyte before and after subjecting the catalyst to the ADTs, see Figure S3. After the degradation test, both the H_{upd} potential region (underpotentially deposited hydrogen, 0.05 – 0.40 V_{RHE}) and the Pt redox potential region (ca. 0.60 – 1.10 V_{RHE}) "shrink" as compared with the CVs of the pristine catalyst. The TEM micrographs of the degraded Pt/C catalysts (see Figure S5) clearly indicate particle growth which can be related to electrochemical Ostwald ripening and / or particle migration and coalescence.[52] Furthermore, particle detachment might occur which is difficult to identify using conventional TEM. Interestingly, the TEM micrographs indicate differences in the degradation behavior between the different bimetallic catalysts. The Pt_xIr_y alloy NPs experience particle growth as well, whereas the Pt – IrO_2 nanocomposites seem to experience less degradation; in particular the Pt + Ir/C catalyst. The results therefore confirm the general ability of IrO_2 to reduce the degradation of Pt/C catalysts. They also indicate differences in the concept between "alloying" and nanocomposites. This becomes even more evident considering the EOT activities.

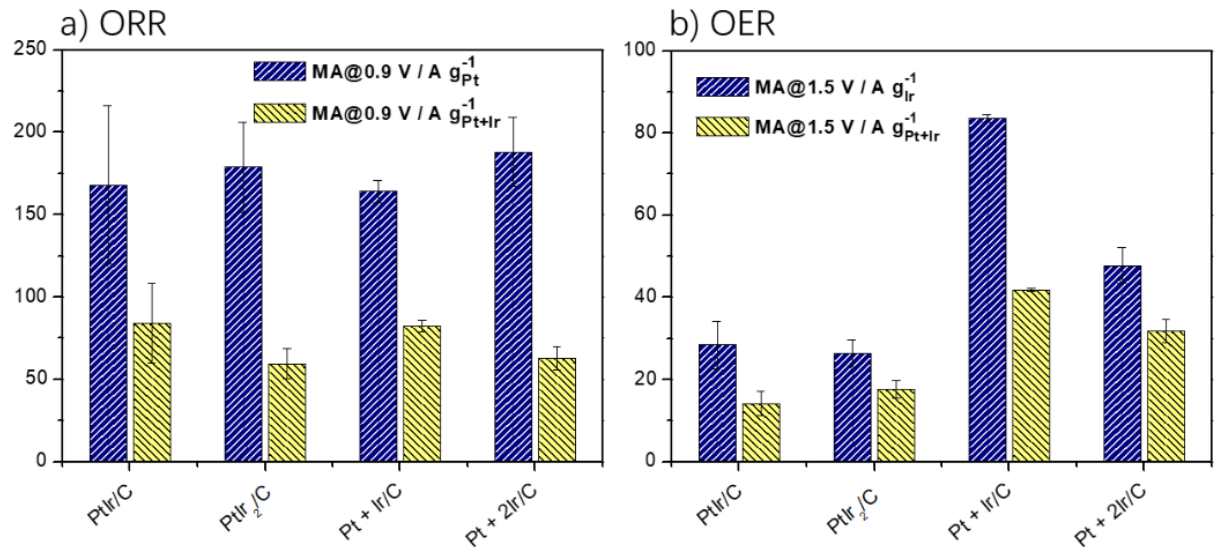

Figure 5. Comparison of the electrochemical mass activity of supported Pt_xIr_y alloy NPs and Pt – IrO_2 nanocomposites after the ADTs. a) ORR performance and b) OER performance. The ORR activity is determined with a scan rate of 50 mV s^{-1} and 1600 rpm applying a potential range of 0.05 - 1.10 V_{RHE}, while the OER activity is determined with a scan rate of 10 mV s^{-1} and 1600 rpm applying a potential range of 1.00 - 1.70 V_{RHE}. As error, the standard deviation from three measurements on different catalyst films is given.

The inflicted change in ORR and OER performance due to the ADTs is summarized in Figure 5. We thereby concentrate on the bifunctional catalysts. After the ADTs, all bifunctional catalysts display a similar ORR mass activity, in particular if the mass activity is based on the (initial) Pt loading. This is in contrast to the results of the pristine catalysts before applying the ADTs reported in Figure 3a where the supported Pt_xIr_y alloy NPs displayed higher mass activities than the supported Pt – IrO_2 nanocomposites. Regarding OER mass activity, the influence of the ADTs is even more pronounced. While the Pt ECSA loss is similar for the supported Pt_xIr_y alloy NPs and the Pt – IrO_2 nanocomposites, a significant difference is detected in OER activity, see Figure 5b. In agreement with the TEM micrographs in Figure S5, the Pt – IrO_2 nanocomposites exhibit a significantly higher mass activity than the supported Pt_xIr_y alloy NPs. The difference between alloy NPs and nanocomposites is most pronounced for the Pt + Ir/C catalyst. After the ADTs, it exhibits the highest OER even though the pristine nanocomposite had a lower OER mass activity than the

supported Pt_xIr_y alloy NPs. The mass activity values after ADTs are 83.6 ± 0.9 A g_{Ir}^{-1} and 41.8 ± 0.4 A g_{Ir+Pt}^{-1}, respectively, whereas the mass activity values for the supported PtIr alloy NPs are only 28.4 ± 5.7 A g_{Ir}^{-1} and 14.2 ± 2.9 A g_{Ir+Pt}^{-1}. That is, the mass activity of the nanocomposite is after the ADTs roughly a factor of three higher than that of the respective alloy NPs, see Table S3 for a complete comparison.

The stabilizing effect of Ir is often discussed in context of a boosted OER activity. That is, the oxidative current forced onto the catalyst is not provided by carbon oxidation but the OER instead. However, IrO_2 is prone to dissolution as well, as it can experience a change in valence state between 3+ and 4+ in a potential range ~0.80 – 1.00 V_{RHE}.[52] A change in valence state requires a current and therefore this process might compete with the OER and carbon corrosion. A rough estimation shows that the currents in each step of the ADT protocol are sufficient to switch the oxidation of ca. half of all Ir atoms in the samples. Our hypothesis to explain the difference in performance degradation between Pt_xIr_y alloy NPs and Pt – IrO_2 nanocomposites is that the stability of IrO_2 is key and that separating IrO_2 from Pt offers significant advantages. In the Pt_xIr_y alloy NPs systems, Pt and Ir are incorporated in the same particle, i.e. once IrO_2 is subjected to degradation inevitably Pt is as well. In the Pt – IrO_2 nanocomposite system, the effect of the ADTs on Pt and Ir can be separated. Thus, the Pt + 2Ir/C catalyst is least affected by the ADTs with respect to ORR performance. Pt is "protected" by IrO_2, however, at the expense of a high relative loss in OER activity. By comparison, in the Pt + Ir/C nanocomposite the Pt NPs are less "protected", and the ORR activity loss is higher, but the OER activity loss is lower. The protective function of IrO_2 comes at least in part from the change in valence state between 3+ and 4+, which requires a charge, but also triggers Ir dissolution.[46]

To substantiate this hypothesis, we analyzed the compositional changes of the catalysts upon applying the ADTs with EDX. As mentioned above, in the pristine Pt – IrO_2 nanocomposites and the PtIr/C, the determined metal composition is close to the nominal value. We confirmed the results also by ICP-MS measurements, see Table S5. Although, the ICP-MS measurements have limitations as discussed in detail in the experimental part *Inductively Coupled Plasma Mass Spectrometry (ICP-MS),* we can follow the Ir and Pt ratio in the catalyst as well as the "washing" supernatant. The results furthermore show that during the "washing" procedure for NP flocculation, only few (less than 4%) NPs are lost into the supernatant. The composition of the pristine $PtIr_2$/C, however, deviates from the nominal one (the Ir / Pt is only 1.21).

The results show that after applying the ADTs, the ratio between Ir and Pt substantially decreases in all bifunctional catalysts. The changes of Ir / Pt before and after degradation test are summarized in Table S4. The results suggest that the increase in IrO_2 in the catalyst leads also to an increase in disproportional Ir loss. Separating Pt and IrO_2 NPs in a nanocomposite allows a fine tuning of the electrochemical properties of the bifunctional catalyst and thus offers advantages for their optimization. The best overall stability and ORR / OER performance is established for the nanocomposite catalysts based on 20 wt. % Pt and 20 wt. % Ir. For this catalyst, minor particle agglomeration is observed after applying ADTs, see Figure S5, and the relative loss of Ir is lowest (see TableS4). Last but not least, the differences between the different catalysts (alloy and nanocomposite) could in part be due to differences in the interaction with the carbon support. However, probing the carbon support in the different catalysts before and after ADT (Figure S6), no significant differences between the catalysts were seen.

Conclusion

Supported monometallic Pt NPs, Pt_xIr_y alloy NPs and Pt – IrO_2 nanocomposites were prepared and measured to investigate ORR / OER performance and stability. The results indicate that the monometallic Pt NPs exhibit the best ORR performance of the investigated catalysts, i.e. the ORR performance is decreased by adding Ir to the catalyst. In case of the nanocomposite catalysts, the results indicate an electronic particle proximity effect between Pt and IrO_2 NPs leading to an increase in oxophilicity of the Pt NPs. The opposite activity trend is found for the OER. The increase in OER activity when introducing Ir to a Pt/C catalyst is accompanied with an increase in stability. Applying an ADT protocol to study the employment of bifunctional Pt – IrO_2 catalysts to mitigate degradation under startup and shutdown, it is seen that the bifunctional catalysts suffer from severe degradation at such challenging conditions. This will also have a direct consequence when applying such catalysts in URFCs in CG configuration when switching between OER and ORR mode and questions their stable long-term operation. In part of the severe degradation might be mitigated by more stable support materials other than carbons, however, the problem of a declining ratio between Ir and Pt most likely will needs to be solved. Last but not least, our results provide evidence that nanocomposite materials show interesting electrochemical properties and might be a suitable strategy to address these stability challenges. Although being far from stable, Pt – IrO_2 nanocomposites allow careful optimization of ORR and OER properties and offer advantages over the conventional approach of alloying Pt and Ir.

Supporting information

The supporting information contains additional experimental data. CVs, CO stripping curves, tables of the specific and mass activities for ORR and OER, ECSA values at beginning and end of the ADTs, a summary of the EDX and ICP-MS data as well as TEM micrographs of the degraded

catalyst. In addition, a summary of Raman data from the catalysts at beginning and end of the ADTs is shown.

Acknowledgements

This work was supported by the Swiss National Science Foundation (SNSF) via the project No. 200021_184742. Jia Du acknowledges funding from the China Scholarship Council (CSC). S. B. Simonsen and L. Theil Kuhn, Technical University of Denmark, are thanked for access to TEM, Tom Vosch for the Raman measurements and Wouter van Beek from the ESRF for measuring XRD on the catalyst samples.

References

(1) She, Z. W.; Kibsgaard, J.; Dickens, C. F.; Chorkendorff, I.; Nørskov, J. K.; Jaramillo, T. F. Combining Theory and Experiment in Electrocatalysis: Insights into Materials Design. *Science*. 2017. https://doi.org/10.1126/science.aad4998.

(2) Peng, L.; Wei, Z. Catalyst Engineering for Electrochemical Energy Conversion from Water to Water: Water Electrolysis and the Hydrogen Fuel Cell. *Engineering*. 2020. https://doi.org/10.1016/j.eng.2019.07.028.

(3) Sievers, G. W.; Jensen, A. W.; Quinson, J.; Zana, A.; Bizzotto, F.; Oezaslan, M.; Dworzak, A.; Kirkensgaard, J. J. K.; Smitshuysen, T. E. L.; Kadkhodazadeh, S.; Juelsholt, M.; Jensen, K. M. Ø.; Anklam, K.; Wan, H.; Schäfer, J.; Čépe, K.; Escudero-Escribano, M.; Rossmeisl, J.; Quade, A.; Brüser, V.; Arenz, M. Self-Supported Pt–CoO Networks Combining High Specific Activity with High Surface Area for Oxygen Reduction. *Nat. Mater.* **2020**. https://doi.org/10.1038/s41563-020-0775-8.

(4) McCrory, C. C. L.; Jung, S.; Ferrer, I. M.; Chatman, S. M.; Peters, J. C.; Jaramillo, T. F. Benchmarking Hydrogen Evolving Reaction and Oxygen Evolving Reaction Electrocatalysts for Solar Water Splitting Devices. *J. Am. Chem. Soc.* **2015**. https://doi.org/10.1021/ja510442p.

(5) Siracusano, S.; Hodnik, N.; Jovanovic, P.; Ruiz-Zepeda, F.; Šala, M.; Baglio, V.; Aricò, A. S. New Insights into the Stability of a High Performance Nanostructured Catalyst for Sustainable Water Electrolysis. *Nano Energy* **2017**.

https://doi.org/10.1016/j.nanoen.2017.09.014.

(6) Carmo, M.; Fritz, D. L.; Mergel, J.; Stolten, D. A Comprehensive Review on PEM Water Electrolysis. *International Journal of Hydrogen Energy*. 2013. https://doi.org/10.1016/j.ijhydene.2013.01.151.

(7) Deng, Y.-J.; Tripkovic, V.; Rossmeisl, J.; Arenz, M. Oxygen Reduction Reaction on Pt Overlayers Deposited onto a Gold Film: Ligand, Strain, and Ensemble Effect. *ACS Catal.* **2016**, *6* (2). https://doi.org/10.1021/acscatal.5b02409.

(8) Whipple, D. T.; Kenis, P. J. A. Prospects of CO2 Utilization via Direct Heterogeneous Electrochemical Reduction. *J. Phys. Chem. Lett.* **2010**. https://doi.org/10.1021/jz1012627.

(9) Dutta, A.; Rahaman, M.; Luedi, N. C.; Mohos, M.; Broekmann, P. Morphology Matters: Tuning the Product Distribution of CO2 Electroreduction on Oxide-Derived Cu Foam Catalysts. *ACS Catal.* **2016**. https://doi.org/10.1021/acscatal.6b00770.

(10) Davies, B. J. V.; Arenz, M.; Rossmeisl, J.; Escudero-Escribano, M. Electrochemical Synthesis of High-Value Chemicals: Detection of Key Reaction Intermediates and Products Combining Gas Chromatography-Mass Spectrometry and in Situ Infrared Spectroscopy. *J. Phys. Chem. C* **2019**, *123* (20). https://doi.org/10.1021/acs.jpcc.9b01017.

(11) Šarić, M.; Davies, B. J. V.; Schjødt, N. C.; Dahl, S.; Moses, P. G.; Escudero-Escribano, M.; Arenz, M.; Rossmeisl, J. Catalyst Design Criteria and Fundamental Limitations in the Electrochemical Synthesis of Dimethyl Carbonate. *Green Chem.* **2019**, *21* (22). https://doi.org/10.1039/c9gc02265a.

(12) Pollet, B. G.; Staffell, I.; Shang, J. L. Current Status of Hybrid, Battery and Fuel Cell Electric Vehicles: From Electrochemistry to Market Prospects. *Electrochimica Acta*. 2012. https://doi.org/10.1016/j.electacta.2012.03.172.

(13) Gangloff, J. J.; Kast, J.; Morrison, G.; Marcinkoski, J. Design Space Assessment of Hydrogen Storage Onboard Medium and Heavy Duty Fuel Cell Electric Trucks. *J. Electrochem. Energy Convers. Storage* **2017**. https://doi.org/10.1115/1.4036508.

(14) Sønderskov, S. H.; Rasmussen, D.; Ilsøe, J.; Blom-Hansen, D.; Munk-Nielsen, S. Detecting Performance Outliers in Fuel Cell Backup Power Systems. In *2019 21st European Conference on Power Electronics and Applications (EPE '19 ECCE Europe)*; 2019; p P.1-P.10. https://doi.org/10.23919/EPE.2019.8915057.

(15) Di Marcoberardino, G.; Chiarabaglio, L.; Manzolini, G.; Campanari, S. A Techno-

Economic Comparison of Micro-Cogeneration Systems Based on Polymer Electrolyte Membrane Fuel Cell for Residential Applications. *Appl. Energy* **2019**. https://doi.org/10.1016/j.apenergy.2019.01.171.

(16) Álvarez Fernández, R.; Corbera Caraballo, S.; Beltrán Cilleruelo, F.; Lozano, J. A. Fuel Optimization Strategy for Hydrogen Fuel Cell Range Extender Vehicles Applying Genetic Algorithms. *Renewable and Sustainable Energy Reviews*. 2018. https://doi.org/10.1016/j.rser.2017.08.047.

(17) Gasteiger, H. A.; Kocha, S. S.; Sompalli, B.; Wagner, F. T. Activity Benchmarks and Requirements for Pt, Pt-Alloy, and Non-Pt Oxygen Reduction Catalysts for PEMFCs. *Applied Catalysis B: Environmental*. 2005. https://doi.org/10.1016/j.apcatb.2004.06.021.

(18) Marković, N. M.; Schmidt, T. J.; Stamenković, V.; Ross, P. N. Oxygen Reduction Reaction on Pt and Pt Bimetallic Surfaces: A Selective Review. *Fuel Cells* **2001**. https://doi.org/10.1002/1615-6854(200107)1:2<105::aid-fuce105>3.3.co;2-0.

(19) Stephens, I. E. L.; Bondarenko, A. S.; Grønbjerg, U.; Rossmeisl, J.; Chorkendorff, I. Understanding the Electrocatalysis of Oxygen Reduction on Platinum and Its Alloys. *Energy and Environmental Science*. 2012. https://doi.org/10.1039/c2ee03590a.

(20) Jia, Q.; Caldwell, K.; Strickland, K.; Ziegelbauer, J. M.; Liu, Z.; Yu, Z.; Ramaker, D. E.; Mukerjee, S. Improved Oxygen Reduction Activity and Durability of Dealloyed PtCox Catalysts for Proton Exchange Membrane Fuel Cells: Strain, Ligand, and Particle Size Effects. *ACS Catal.* **2015**. https://doi.org/10.1021/cs501537n.

(21) Antolini, E.; Salgado, J. R. C.; Giz, M. J.; Gonzalez, E. R. Effects of Geometric and Electronic Factors on ORR Activity of Carbon Supported Pt-Co Electrocatalysts in PEM Fuel Cells. *Int. J. Hydrogen Energy* **2005**. https://doi.org/10.1016/j.ijhydene.2005.05.001.

(22) Kuriganova, A. B.; Leont'ev, I. N.; Smirnova, N. V. PtIr/C Catalysts Synthesized by Electrochemical Dispersion Method for Proton Exchange Membrane Fuel Cells. *Russ. J. Electrochem.* **2018**, *54* (6), 561–565. https://doi.org/10.1134/S1023193518060113.

(23) Carmo, M.; Keeley, G. P.; Holtz, D.; Grube, T.; Robinius, M.; Müller, M.; Stolten, D. PEM Water Electrolysis: Innovative Approaches towards Catalyst Separation, Recovery and Recycling. *Int. J. Hydrogen Energy* **2019**. https://doi.org/10.1016/j.ijhydene.2018.12.030.

(24) Ali, I.; AlGhamdi, K.; Al-Wadaani, F. T. Advances in Iridium Nano Catalyst Preparation,

Characterization and Applications. *Journal of Molecular Liquids*. 2019. https://doi.org/10.1016/j.molliq.2019.02.050.

(25) Spöri, C.; Kwan, J. T. H.; Bonakdarpour, A.; Wilkinson, D. P.; Strasser, P. The Stability Challenges of Oxygen Evolving Catalysts: Towards a Common Fundamental Understanding and Mitigation of Catalyst Degradation. *Angew. Chemie Int. Ed.* **2017**, *56* (22), 5994–6021. https://doi.org/https://doi.org/10.1002/anie.201608601.

(26) Altmann, S.; Kaz, T.; Friedrich, K. A. Bifunctional Electrodes for Unitised Regenerative Fuel Cells. *Electrochim. Acta* **2011**. https://doi.org/10.1016/j.electacta.2011.01.077.

(27) Sadhasivam, T.; Dhanabalan, K.; Roh, S. H.; Kim, T. H.; Park, K. W.; Jung, S.; Kurkuri, M. D.; Jung, H. Y. A Comprehensive Review on Unitized Regenerative Fuel Cells: Crucial Challenges and Developments. *International Journal of Hydrogen Energy*. 2017. https://doi.org/10.1016/j.ijhydene.2016.10.140.

(28) Regmi, Y. N.; Peng, X.; Fornaciari, J. C.; Wei, M.; Myers, D. J.; Weber, A. Z.; Danilovic, N. A Low Temperature Unitized Regenerative Fuel Cell Realizing 60% Round Trip Efficiency and 10 000 Cycles of Durability for Energy Storage Applications. *Energy Environ. Sci.* **2020**, *13* (7), 2096–2105. https://doi.org/10.1039/C9EE03626A.

(29) Ioroi, T.; Kitazawa, N.; Yasuda, K.; Yamamoto, Y.; Takenaka, H. Iridium Oxide/Platinum Electrocatalysts for Unitized Regenerative Polymer Electrolyte Fuel Cells. *J. Electrochem. Soc.* **2000**. https://doi.org/10.1149/1.1393478.

(30) Ioroi, T.; Yasuda, K. Platinum-Iridium Alloys as Oxygen Reduction Electrocatalysts for Polymer Electrolyte Fuel Cells. *J. Electrochem. Soc.* **2005**, *152* (10), A1917. https://doi.org/10.1149/1.2006547.

(31) Yao, W.; Yang, J.; Wang, J.; Nuli, Y. Chemical Deposition of Platinum Nanoparticles on Iridium Oxide for Oxygen Electrode of Unitized Regenerative Fuel Cell. *Electrochem. commun.* **2007**. https://doi.org/10.1016/j.elecom.2006.12.017.

(32) Godínez-Salomón, F.; Albiter, L.; Mendoza-Cruz, R.; P. Rhodes, C. Bimetallic Two-Dimensional Nanoframes: High Activity Acidic Bifunctional Oxygen Reduction and Evolution Electrocatalysts. *ACS Appl. Energy Mater.* **2020**, *3* (3), 2404–2421. https://doi.org/10.1021/acsaem.9b02051.

(33) Ioroi, T.; Kitazawa, N.; Yasuda, K.; Yamamoto, Y.; Takenaka, H. IrO2-Deposited Pt Electrocatalysts for Unitized Regenerative Polymer Electrolyte Fuel Cells. *J. Appl.*

Electrochem. **2001**. https://doi.org/10.1023/A:1012755809488.

(34) Moriau, L. J.; Bele, M.; Vižintin, A.; Ruiz-Zepeda, F.; Petek, U.; Jovanovič, P.; Šala, M.; Gaberšček, M.; Hodnik, N. Synthesis and Advanced Electrochemical Characterization of Multifunctional Electrocatalytic Composite for Unitized Regenerative Fuel Cell. *ACS Catal.* **2019**. https://doi.org/10.1021/acscatal.9b03385.

(35) da Silva, G. C.; Mayrhofer, K. J. J.; Ticianelli, E. A.; Cherevko, S. Dissolution Stability: The Major Challenge in the Regenerative Fuel Cells Bifunctional Catalysis. *J. Electrochem. Soc.* **2018**. https://doi.org/10.1149/2.1201816jes.

(36) Speder, J.; Altmann, L.; Roefzaad, M.; Bäumer, M.; Kirkensgaard, J. J. K.; Mortensen, K.; Arenz, M. Pt Based PEMFC Catalysts Prepared from Colloidal Particle Suspensions-a Toolbox for Model Studies. *Phys. Chem. Chem. Phys.* **2013**, *15* (10). https://doi.org/10.1039/c3cp50195g.

(37) Neumann, S.; Grotheer, S.; Tielke, J.; Schrader, I.; Quinson, J.; Zana, A.; Oezaslan, M.; Arenz, M.; Kunz, S. Nanoparticles in a Box: A Concept to Isolate, Store and Re-Use Colloidal Surfactant-Free Precious Metal Nanoparticles. *J. Mater. Chem. A* **2017**, *5* (13). https://doi.org/10.1039/c7ta00628d.

(38) Quinson, J.; Inaba, M.; Neumann, S.; Swane, A. A.; Bucher, J.; Simonsen, S. B.; Theil Kuhn, L.; Kirkensgaard, J. J. K.; Jensen, K. M.; Oezaslan, M.; Kunz, S.; Arenz, M. Investigating Particle Size Effects in Catalysis by Applying a Size-Controlled and Surfactant-Free Synthesis of Colloidal Nanoparticles in Alkaline Ethylene Glycol: Case Study of the Oxygen Reduction Reaction on Pt. *ACS Catal.* **2018**, *8* (7). https://doi.org/10.1021/acscatal.8b00694.

(39) Quinson, J.; Neumann, S.; Wannmacher, T.; Kacenauskaite, L.; Inaba, M.; Bucher, J.; Bizzotto, F.; Simonsen, S. B.; Theil Kuhn, L.; Bujak, D.; Zana, A.; Arenz, M.; Kunz, S. Colloids for Catalysts: A Concept for the Preparation of Superior Catalysts of Industrial Relevance. *Angew. Chemie - Int. Ed.* **2018**, *57* (38). https://doi.org/10.1002/anie.201807450.

(40) Spanos, I.; Rellán, C. P.; Altmann, L.; Bäumer, M.; Arenz, M. Pt<inf>x</Inf>Co<inf>1-X</Inf> Alloy NPs Prepared by Colloidal Tool-Box Synthesis: The Effect of de-Alloying on the Oxygen Reduction Reaction Activity. *Int. J. Hydrogen Energy* **2014**, *39* (17). https://doi.org/10.1016/j.ijhydene.2014.03.199.

(41) Bucher, J.; Quinson, J.; Mingers, A. M.; Zhang, D.; Arenz, M. On the Facile and Accurate Determination of the Pt Content in Standard Carbon Supported Pt Fuel Cell Catalysts. *Anal. Chim. Acta* **2020**, *1101*. https://doi.org/10.1016/j.aca.2019.12.010.

(42) Bizzotto, F.; Quinson, J.; Zana, A.; Kirkensgaard, J. J. K.; Dworzak, A.; Oezaslan, M.; Arenz, M. Ir Nanoparticles with Ultrahigh Dispersion as Oxygen Evolution Reaction (OER) Catalysts: Synthesis and Activity Benchmarking. *Catal. Sci. Technol.* **2019**, *9* (22). https://doi.org/10.1039/c9cy01728c.

(43) Inaba, M.; Quinson, J.; Bucher, J. R.; Arenz, M. On the Preparation and Testing of Fuel Cell Catalysts Using the Thin Film Rotating Disk Electrode Method. *J. Vis. Exp.* **2018**, *2018* (133). https://doi.org/10.3791/57105.

(44) Mayrhofer, K. J. J.; Strmcnik, D.; Blizanac, B. B.; Stamenkovic, V.; Arenz, M.; Markovic, N. M. Measurement of Oxygen Reduction Activities via the Rotating Disc Electrode Method: From Pt Model Surfaces to Carbon-Supported High Surface Area Catalysts. *Electrochim. Acta* **2008**, *53* (7). https://doi.org/10.1016/j.electacta.2007.11.057.

(45) Alia, S. M.; Hurst, K. E.; Kocha, S. S.; Pivovar, B. S. Mercury Underpotential Deposition to Determine Iridium and Iridium Oxide Electrochemical Surface Areas. *J. Electrochem. Soc.* **2016**, *163* (11), F3051–F3056. https://doi.org/10.1149/2.0071611jes.

(46) Gómez, R.; Weaver, M. J. Electrochemical Infrared Studies of Monocrystalline Iridium Surfaces. Part 2: Carbon Monoxide and Nitric Oxide Adsorption on Ir(110). *Langmuir* **1998**, *14* (9), 2525–2534. https://doi.org/10.1021/la9711692.

(47) Crowtz, T. C.; Dahn, J. R. Screening Bifunctional Pt Based NSTF Catalysts for Durability with the Rotating Disk Electrode: The Effect of Ir and Ru. *J. Electrochem. Soc.* **2018**. https://doi.org/10.1149/2.0891810jes.

(48) Chang, C. H.; Yuen, T. S.; Nagao, Y.; Yugami, H. Electrocatalytic Activity of Iridium Oxide Nanoparticles Coated on Carbon for Oxygen Reduction as Cathode Catalyst in Polymer Electrolyte Fuel Cell. *J. Power Sources* **2010**. https://doi.org/10.1016/j.jpowsour.2010.01.049.

(49) Nesselberger, M.; Roefzaad, M.; Fayçal Hamou, R.; Ulrich Biedermann, P.; Schweinberger, F. F.; Kunz, S.; Schloegl, K.; Wiberg, G. K. H.; Ashton, S.; Heiz, U.; Mayrhofer, K. J. J.; Arenz, M. The Effect of Particle Proximity on the Oxygen Reduction Rate of Size-Selected Platinum Clusters. *Nat. Mater.* **2013**, *12* (10).

https://doi.org/10.1038/nmat3712.

(50) Speder, J.; Altmann, L.; Bäumer, M.; Kirkensgaard, J. J. K.; Mortensen, K.; Arenz, M. The Particle Proximity Effect: From Model to High Surface Area Fuel Cell Catalysts. *RSC Adv.* **2014**, *4* (29). https://doi.org/10.1039/c4ra00261j.

(51) Sandbeck, D. J. S.; Secher, N. M.; Inaba, M.; Quinson, J.; Sørensen, J. E.; Kibsgaard, J.; Zana, A.; Bizzotto, F.; Speck, F. D.; Paul, M. T. Y.; Dworzak, A.; Dosche, C.; Oezaslan, M.; Chorkendorff, I.; Arenz, M.; Cherevko, S. The Dissolution Dilemma for Low Pt Loading Polymer Electrolyte Membrane Fuel Cell Catalysts. August 27, 2020. https://doi.org/10.26434/chemrxiv.12866672.v1.

(52) da Silva, G. C.; Mayrhofer, K. J. J.; Ticianelli, E. A.; Cherevko, S. The Degradation of Pt/IrOx Oxygen Bifunctional Catalysts. *Electrochim. Acta* **2019**. https://doi.org/10.1016/j.electacta.2019.04.017.

(53) Nørskov, J. K.; Rossmeisl, J.; Logadottir, A.; Lindqvist, L.; Kitchin, J. R.; Bligaard, T.; Jónsson, H. Origin of the Overpotential for Oxygen Reduction at a Fuel-Cell Cathode. *J. Phys. Chem. B* **2004**. https://doi.org/10.1021/jp047349j.

(54) Reier, T.; Oezaslan, M.; Strasser, P. Electrocatalytic Oxygen Evolution Reaction (OER) on Ru, Ir, and Pt Catalysts: A Comparative Study of Nanoparticles and Bulk Materials. *ACS Catal.* **2012**. https://doi.org/10.1021/cs3003098.